

Application of a serial extended forecast experiment using the ECMWF model to interpret the predictive skill of tropical intraseasonal variability

P. A. Agudelo · C. D. Hoyos · P. J. Webster · J. A. Curry

Received: 13 November 2007 / Accepted: 8 July 2008
© Springer-Verlag 2008

Abstract The extended-range forecast skill of the ECMWF operational forecast model is evaluated during tropical intraseasonal oscillation (ISO) events in the Indo-West Pacific warm pool. The experiment consists of ensemble extended serial forecasts including winter and summer ISO cases. The forecasts are compared with the ERA-40 analyses. The analysis focuses on understanding the origin of forecast errors by studying the vertical structure of relevant dynamical and moist convective features associated with the ISO. The useful forecast time scale for circulation anomalies is in average 13 days during winter compared to 7–8 days during summer. The forecast skill is not stationary and presents evidence of a flow-dependent nature, with states of the coupled system corresponding to long-lived convective envelopes associated with the ISO for which the skill is always low regardless of the starting date of the forecast. The model is not able to forecast skillfully the generation of specific humidity anomalies and results indicate that the convective processes in the model are associated with the erosion of the ISO forecast skill in the model. Circulation-associated anomalies are forecast better than moist convective associated anomalies. The model tends to generate a more stable atmosphere, limiting the model's capability to reproduce deep convective events, resulting in smaller humidity and circulation anomalies in the forecasts compared to those in ERA-40.

Keywords Intraseasonal oscillation · Madden–Julian oscillation · Asian monsoon · Forecasting skill · Numerical modeling

1 Introduction

Understanding, modeling, and forecasting intraseasonal oscillations (ISOs) in the Indo-West Pacific warm pool and its effects on regional weather and global climate remains a significant challenge for the scientific community (e.g. Lau and Waliser 2005; Zhang 2005). In general, the tropical ISO exhibits a rich and coherent vertical structure in the atmosphere on a time scale of 30–80 days, with low-level moisture convergence and upper tropospheric divergence anomalies (e.g. Sperber 2003). Through interaction with the upper ocean, ISOs lead to moistening of the boundary layer and the development of shallow convection, often followed by a gradual and then more rapid moistening of the middle troposphere with the onset of deep convection (e.g. Stephens et al. 2004; Agudelo et al. 2006; Tian et al. 2006).

In general, the ISO is strongest during the boreal winter and spring seasons when it appears as a predominantly eastward propagating large-scale system of convection along the equator, extending from the Indian Ocean East to the dateline (e.g. Hendon and Salby 1994). During the south Asian summer monsoon season, the ISO is typically weaker but of a more complex character (e.g. Madden 1986; Lawrence and Webster 2002; Hoyos and Webster 2007). This marked seasonality is evident in the differences in amplitude, frequency, and propagation features between boreal summer and winter. The main difference between the winter and summer ISO is the northward propagation of convective anomalies over the Indian Ocean during summer, which is not present during winter.

P. A. Agudelo (✉) · C. D. Hoyos · P. J. Webster · J. A. Curry
School of Earth and Atmospheric Sciences,
Georgia Institute of Technology, 311 Ferst Drive,
Atlanta, GA 30332-0340, USA
e-mail: pagudelo@eas.gatech.edu

Accurate tropical ISO forecasts are essential for extended-range predictions of wet and dry spells during the Australian (e.g. Hendon and Liebmann 1990) and southeast Asian monsoons (e.g. Webster and Hoyos 2004), extra-tropical weather (e.g. Ferranti et al. 1990), and hurricane activity (e.g. Maloney and Hartmann 2000). However, many attempts to simulate and forecast the ISO using numerical models have failed to reproduce its characteristics or to obtain realistic propagation speeds (e.g. Slingo et al. 1996; Lin et al. 2006). Slingo et al. (1996) found that none of the atmosphere, only general circulation models (GCMs) in the Atmospheric Model Intercomparison Project were able to capture the spectral peak associated with the Madden–Julian oscillation (MJO; eastward propagating ISO, e.g. Madden and Julian 1994; Zhang 2005). Lin et al. (2006) evaluated tropical intraseasonal variability in 14 GCMs and showed that current state-of-the-art GCMs have significant problems in simulating tropical intraseasonal variability, with typically very weak total intraseasonal variance of precipitation often less than half of the observed value. Lin et al. (2006) also found a lack of coherent eastward propagation of the MJO as well as an over-reddened precipitation spectrum, associated with persistence of equatorial precipitation. An additional problem is the weak precipitation variance in the MJO wavenumber-frequency band in spite of the fact that many of these models have reasonable values of zonal wind variance.

Previous studies of medium and extended-range forecast skill (e.g. Chen and Alpert 1990; Lau and Chang 1992; Jones et al. 2000) suggest that the useful forecast limit of filtered upper-level velocity potential is about 8 days in the tropics. Also, in general, the forecasting skill of ISO anomalies of numerical weather prediction (NWP) models is less than that of statistical prediction techniques (e.g. Waliser et al. 1999; Wheeler and Weickmann 2001; Webster and Hoyos 2004). The main goals of this study are to evaluate the extended-range forecast skill of a state-of-the-art operational NWP model, and to identify the main reasons for the poor forecast skill in the context of observed ISO/MJO events.

Observational analyses of the large-scale three dimensional structure and spatial–temporal evolution of the ISO have allowed possible causes of the ISO simulation and forecast difficulties to be identified (e.g. Tian et al. 2006; Hendon and Liebmann 1990; Lin and Johnson 1996; Kemball-Cook and Weare 2001; Kiladis et al. 2005). However, most studies on the simulation and forecasting skill of the ISO have been restricted to the analysis of 2-dimensional fields in the horizontal plane (e.g. Slingo et al. 1996; Lin et al. 2006; Chen and Alpert 1990), with the exception of Sheng (1995), Gustafson and Weare (2004) and Drbohlav and Wang (2007) who have studied the

simulation, but not the forecasts skill, of the horizontal and vertical structure of the ISO.

Here we use a systematic approach to examine, not only the horizontal structure of the forecast ISO in the Indo-West Pacific basin, but also the vertical structure of the atmospheric anomalies. We evaluate the forecasts of regional and local vertical structure of ISO-related anomalies from a numerical experiment using the European centre for medium-range weather forecasts (ECWMF) coupled model using results from the ECMWF operational atmospheric analysis/reanalysis system (ERA-40, Simmons and Gibson 2000; Uppala et al. 2005) data. The skill of the coupled model in simulating ISOs is evaluated at different stages of convective activity (suppressed, transition and active) by using an experimental design based on serial simulations that are initialized at different stages of the ISO. The use of an operational forecast model with an active data assimilation system for the serial runs experiment rather than a GCM run in climate mode provides a more accurate measure of the ISO forecast skill, allowing direct comparison with observations. Numerical models are often tested for their ability to simulate the spectral characteristics of intraseasonal variability from individual long-term runs. While this type of analysis provides information about the ISO simulation skill of a particular model, it is not useful to estimate the actual forecast skill of the same model. The serial runs experiment allows a direct assessment of the overall medium-range forecast skill considering forecasts starting in all phases of the MJO by comparing the forecast with an observed event.

This analysis explores numerical predictions of the ISO observed during the intensive observing period (IOP) of the tropical ocean global atmosphere (TOGA) coupled ocean–atmosphere response experiment (COARE, Webster and Lukas 1992), which took place over the West Pacific warm pool during the 1992/1993 winter. In addition, significant ISO events during the summers of 2002 and 2004 are also analyzed. Considering summer cases is important since most studies only address the winter ISO. An experimental design is used whereby serial forecasts are made for a period of 30 days, over the life cycle of the ISO. Other studies have used the same experimental framework (Agudelo et al. 2006; Woolnough et al. 2007; Vitart et al. 2007). In contrast to the Woolnough et al. (2007) and Vitart et al. (2007) studies, which estimated the skill of the forecast by projecting the forecasts onto two multivariate EOF modes that represent the winter MJO and comparing the forecast with the observed principal components, our analysis is focused on identifying the origin of the errors in the forecast. This manuscript is organized as follows: Sect. 2 describes the numerical experiment and data analysis. Section 3 presents the analyses of the skill of the ECMWF model in forecasting the vertical structure of the ISO

during winter and summer cases. Discussions and conclusions are given in Sect. 4.

2 Numerical experiment design and analysis

The numerical experiments used in this study are part of a series of extended-range forecast simulations conducted jointly between ECMWF and Georgia Tech. The experiments emerged as a major recommendation from the 2003 ECMWF/CLIVAR intraseasonal variability workshop (ECMWF 2004) that were designed to evaluate the ability of the ECMWF coupled model to reproduce observations during different phases of the ISO for some well documented events. The experiment is similar in philosophy to the NMC/NOAA dynamic extended-range forecast (DERF: Tracton et al. 1989) experiments conducted in the 1980s. The DERF experiment considered sets of 10-day forecasts initialized each day consecutively, for 30 days. These experiments allowed a detailed study of error growth and propagation as a function of time (Reynolds et al. 1994). As part of the ECMWF experiment, a series of 30-day forecast integrations (extended forecast runs) were completed for selected ISO cases during both boreal summer and winter. The series of integrations commenced every day during the duration of the lifecycle of each of the identified events, for a period between ~20 and 25 days before and after the maximum convection in the West Pacific Warm Pool or Central Indian Ocean, depending on the case (see Fig. 1 for a schematic diagram). The integrations include a control forecast and four ensemble members. Interpreting the forecast results relative to when the model was initialized in reference to the ISO lifecycle provides a basis for objectively discerning when and how the ECMWF model loses skill forecasting intraseasonal activity.

The forecasts were performed using the fully-coupled ECMWF model in the monthly forecasting framework (Vitart 2004). Woolnough et al. (2007) and Vitart et al. (2007) suggest that while the ECMWF atmospheric only model can produce a reasonable ISO, the coupled model integrations shows improvement in the forecast skill. In addition several studies have shown that the ISO originates as a result of atmosphere–ocean interaction. Therefore, incorporating the coupled processes would seem to be necessary to improve the simulation of ISO in terms of their intensity, propagation, and seasonality as suggested by a number of studies (e.g. Wang and Xie 1998; Waliser et al. 1999; Woolnough et al. 2000; Webster et al. 2002; Fu et al. 2003; Inness et al. 2003; Fu and Wang 2004; Kim et al. 2008). These studies suggest that the intraseasonal variability of sea surface temperature plays a determining role in the evolution of the MJO/ISO. It is for this reason that it is vital to use a coupled model for the present study.

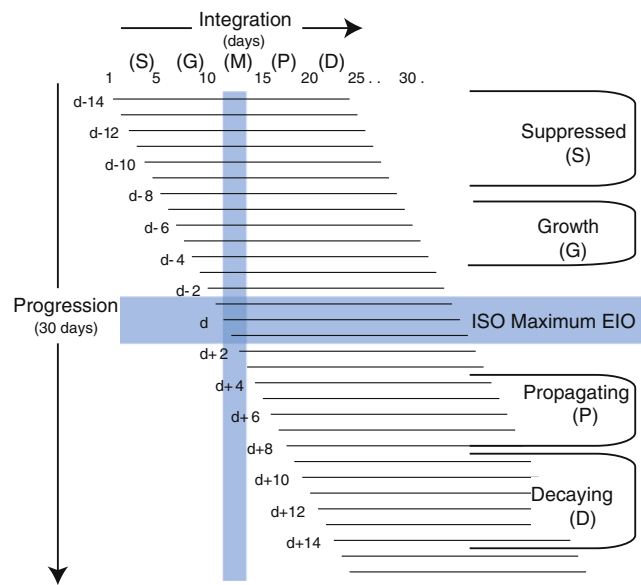


Fig. 1 Schematic diagram of the extended serial integrations. *Blue regions* show the timing of the maximum amplitude of the ISO (*M*) in a specified region between the suppressed (*S*), growth (*G*), propagating (*P*) and decaying (*D*) phases of the event

The atmospheric component of the coupled model is the ECMWF atmospheric model integrated forecast system (IFS). The model used in this study has a nominal horizontal resolution of 1.9×1.9 degrees (TL95) with 40 levels in the vertical. The oceanic component is the Max Plank Institute hamburg ocean primitive equation (HOPE) model which has a zonal resolution of 1.4 degrees, a meridional resolution of 0.3 degrees at the equator and 1.4 at the extratropics, and 29 vertical levels with 10 m resolution in the upper 100 m (Wolff et al. 1997). The coupling of the components is through the interface ocean–atmosphere sea ice soil (OASIS) platform (Terray et al. 1995). Initial conditions for the atmospheric and land surface were obtained from the ERA-40. The ECMWF oceanic data assimilation system provided initial conditions for the oceanic component (Balmaseda et al. 2005). Each ensemble member was generated by slightly perturbing the initial atmospheric and oceanic conditions in the same way as in the EMCWF monthly forecasting system (Vitart 2004; Vialard et al. 2003) using a singular vectors method (Buizza and Palmer 1995). In addition, model tendencies from the atmospheric physics are randomly perturbed every time step throughout the integrations to account for the effects of uncertainties in the model subgrid-scale parameterizations (Buizza et al. 1999). The control forecast is run without perturbations. Perturbations of the system do not target the MJO and are mainly in the extratropics and in some tropical areas targeting tropical cyclones (Puri et al. 2001).

The forecast skill is evaluated by studying relevant dynamical and moist convective features associated with

the ISO relative to the ERA-40 analysis of the ISO. We focus on the tropospheric vertical structure associated with the ISO in the Indo-West Pacific region, estimating the pattern (or spatial) correlation and the standardized pattern root-mean-squared (RMS) error of 5-day moving average anomalies of longitude- and latitude-height snapshots. Using a 5-day moving average filters out high-frequency variability that could potentially mask the estimation of the skill of the extended forecast. In this manner we concentrate on the ISO low frequency envelope rather than the rapidly changing characteristics of convection. We estimate the regional-averaged correlation and RMS error of outgoing longwave radiation (OLR), and 200 and 850 hPa winds. Correlation and RMS error are calculated for different lead times in order to evaluate the degree of covariability (i.e. phasing) between the model results and the observations as well as the deviation of the integrations from the observations (absolute error), respectively. Anomalies of zonal and meridional winds, specific humidity and OLR are selected as the variables most representative of the vertical structure of the ISO since they summarize the circulation and convective anomalies that occur during an ISO event. The spread of the ensemble members is also evaluated as it is an important measure of predictability. The amplitude of the intraseasonal spectral band is also evaluated by comparing observations with integrations at different lead times. The joint probability density function (PDF) between observations and forecasts and the spatial structure of the skill of the forecast (correlation and RMS maps for different lead times) are also constructed.

3 Forecast skill of ISO-related anomalies

In order to explore potential seasonal differences in extended-range forecast skill of the model, we consider both winter and summer ISO events.

3.1 Winter case: TOGA-COARE

Two eastward propagating ISO events starting over the Indian Ocean and moving toward the West Pacific occurred during the TOGA-COARE experiment with intensified rainfall during the last two weeks of December 1992 and between late January and early February 1993. We concentrate initially on the analysis of the zonal vertical structure of the two ISO events during the 1992–1993 winter in an equatorial strip in the Indo-West Pacific region between 60°E and 170°W and from 1,000 to 100 hPa. We computed latitudinally-averaged zonal winds and specific humidity anomalies in the 10°S–10°N latitude band relative to the mean during the TOGA-COARE experiment

(in particular the mean between December 1, 1992 and January 31, 1993). Correlations and standardized RMS error between model forecasts and ERA-40 were calculated. The standardized RMS error was estimated for 5-day averaged anomalies of zonal winds and specific humidity, for every day of the 30 day forecasts, as the mean square root of the squared differences between ERA-40 and forecasts, divided by the standard deviation of the ERA-40 in the same period. The correlation and the RMS error were estimated for the control forecast and each ensemble member. By definition, when the standardized RMS error is greater than 1, the error in the forecast is greater than the variability of the data.

From the winter serial experiment we have forecasts ranging from 1-day to 30-day lead times, starting from 62 different consecutive days (from December 1, 1992 to January 31, 1993), allowing us to study the behavior of the forecast skill relative to the initial conditions and for different forecast lead times. Figures 2a, b and 3a, b show a forecast lead time—start of the forecast diagram of pattern correlation and standardized RMS error for the control run for zonal winds and specific humidity in the Indo-West Pacific region (10°S–10°N, 60°E–170°W), respectively. Figures 2c, d and 3c, d show the average pattern correlation and RMS error, which provide an estimation of the overall forecast skill of the model, for each forecast lead time for the control forecast and each ensemble member. The pattern correlation and standardized RMS error of the vertical structure (from 1,000 to 200 hPa) of atmospheric anomalies are estimated using 6 levels: 200, 500, 700, 850, 925, and 1,000 hPa.

As expected, the average forecast skill of the vertical structure of the anomalies (correlation and RMS error) for the control forecast and each ensemble member, which appears remarkably similar among all runs, show that the closer to the 30-day forecast the model becomes, on average, less skillful than at the beginning of the forecast period. However, the skill of the model is far from stationary, showing structured variability over time. The changes in skill from one day to the next do not appear to be random as could be expected from a perfect model or for a totally unpredictable system but rather appear to depend strongly both on the initial conditions and the atmospheric environment to be forecast. This, a common feature shared by Figs. 2 and 3, indicates the flow-dependent nature of the predictability and forecast skill of the ocean–atmosphere system (Palmer et al. 2005). Due to the nonlinearity of the equations of motion, in combination with the parameterized processes, there are regions of the attractor where uncertainties grow faster than in others. Such dependence is present in all ensemble members as suggested by the similar behavior of the correlation and standardized RMS error for different extended forecast lead times among all

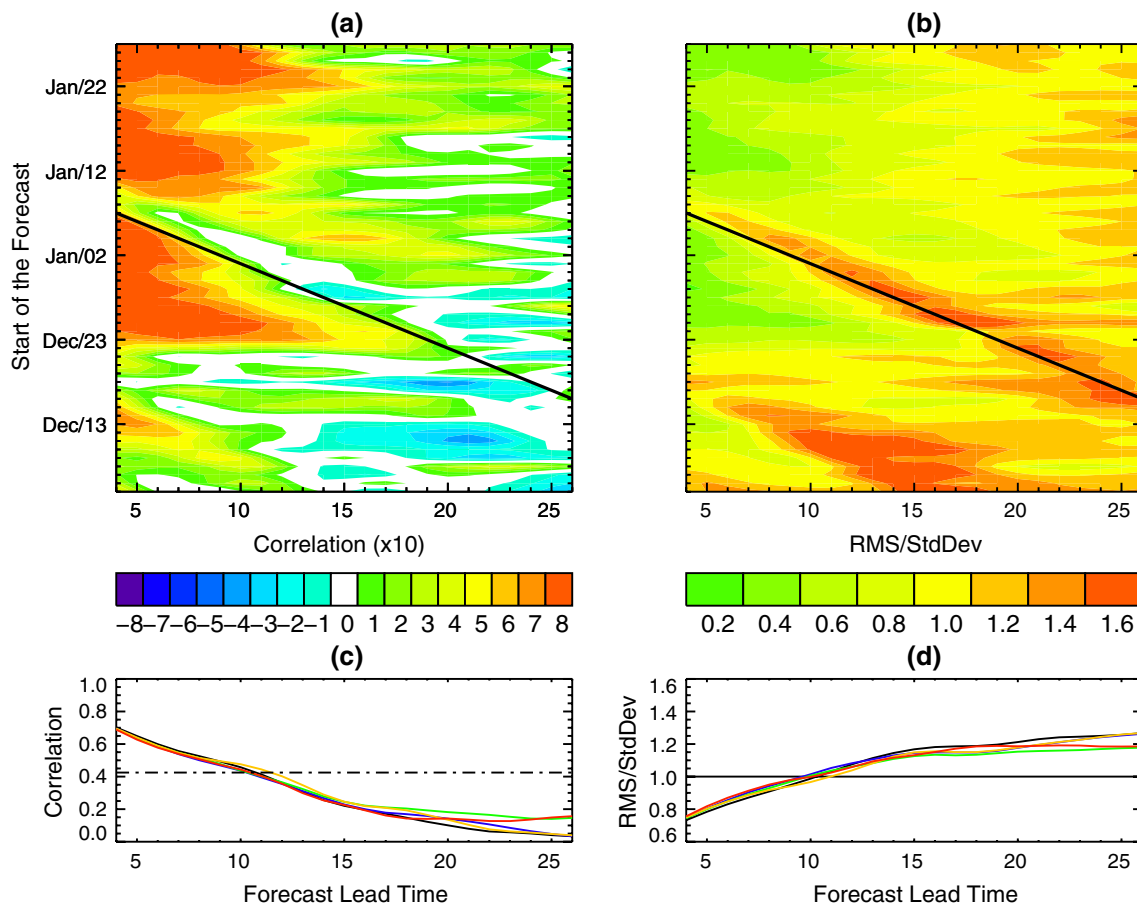


Fig. 2 Distribution of the **a** correlation and **b** standardized RMS for the control run as a function of forecast lead time and start of the forecast for vertical anomalies of zonal winds in the Indo-West Pacific region (10°S–10°N, 60°E–170°W) for the TOGA-COARE case. *Black line* corresponds to the forecast of January 11, 1993 from

different lead times. Average **c** correlation and **d** RMS error estimated from the vertical structure of the anomalies from 1000 to 200 hPa for the control run (*black line*) and all ensemble members (*color lines*). *Dash-dotted line* corresponds to the 99% statistical significance threshold. Significance was estimated using Student's *t*-test

members (Figs. 2c, d and 3c, d). While the set of ensembles is small, the fact that the skill of all members is similar in all runs suggests that the spread of the ensembles is not large enough to account for all degrees of freedom in the coupled system.

The diagonal patterns observed in Figs. 2 and 3, which always occur around a specific forecast date, indicate that there are states of the system for which the skill of the forecast is always low. As an example, the diagonal black lines in Figs. 2 and 3 correspond to the forecast of January 11, 1993 from different lead times. This line is associated with low values of correlation and high values of RMS error in both zonal winds and specific humidity. Thus, irrespective of the timing of the start of the forecast, the regional skill of the model is low for a forecast targeted around January 11, 1993. The conditions around this particular date (January 11, 1993) appear to be of a transitional and active nature. Figure 4 shows the 10-day forecast of

latitudinally-averaged specific humidity in the Indo-West Pacific region for January 11, 1993 to January 13, 1993. ERA-40 anomalies (top) show the growth of the convective event starting in the Indian Ocean. The three control forecasts (bottom) suggest a drier atmosphere than ERA-40 data. As can be seen in Fig. 4, the model forecast a positive specific humidity anomaly in the right location (~70°E) but not sufficiently deep, missing the convective event. In general, the results indicate that the model tends to forecast a drier atmosphere compared to ERA-40 analyses. One of the reasons for the model's poor extended-range forecast skill is that the amplitude of the forecast 5-day averaged anomalies is considerably lower than that found in the ERA-40.

While there is low skill in the 10-day specific humidity forecast, in particular around convective events, zonal wind forecasts for 5-day average anomalies are still useful at the same lead time. In some cases and even for short lead

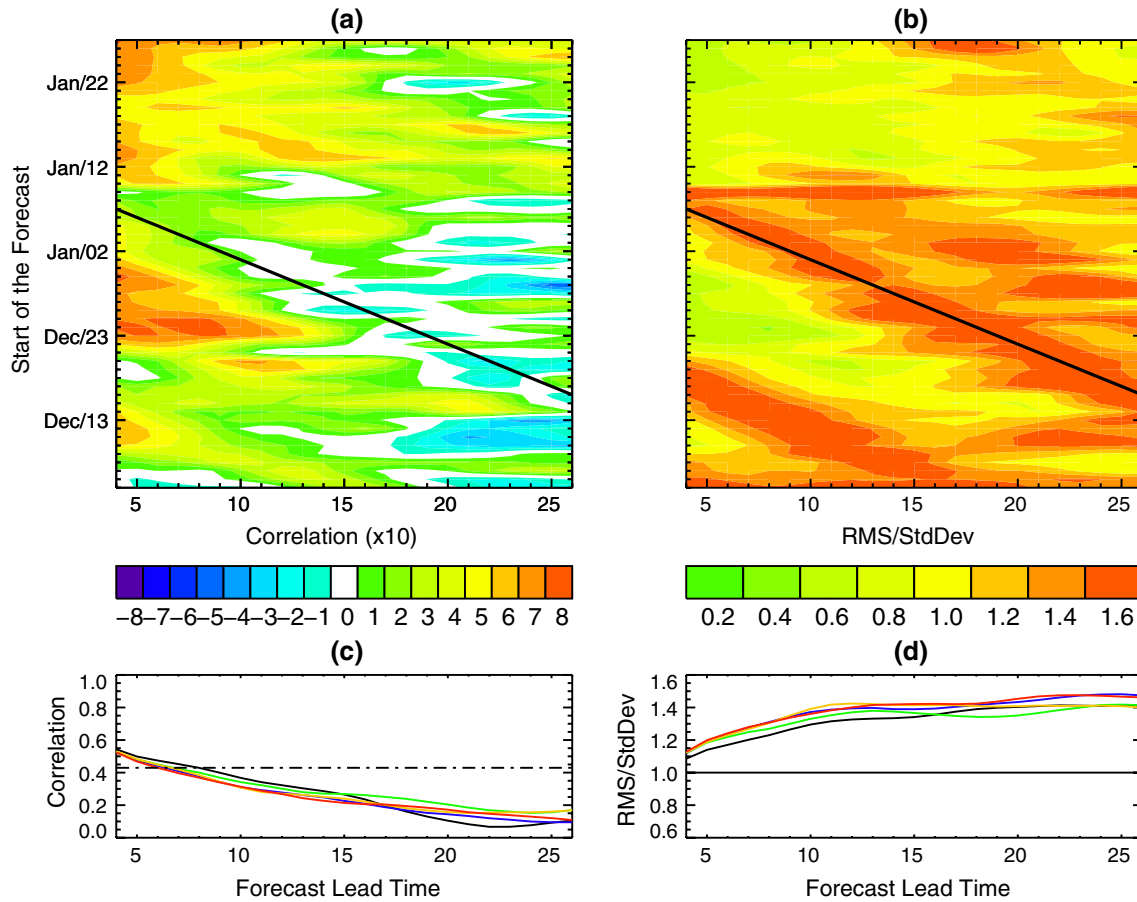


Fig. 3 Same as Fig. 1 but for specific humidity

times, while the forecast specific humidity pattern seems to correlate well with observations (e.g. 0.66 for 4-lead time), the standardized RMS is already higher than 1 (1.10).

Figure 5 shows the ERA-40 data and 10-day control forecasts of zonal winds and specific humidity in the Indo-

West Pacific region for January 16, 1993, which corresponds to a more mature convective stage of the event presented in Fig. 4. In this case, the skill of the zonal wind forecast is relatively good (correlation 0.78, RMS error 0.71). The pattern of the forecast zonal wind anomalies

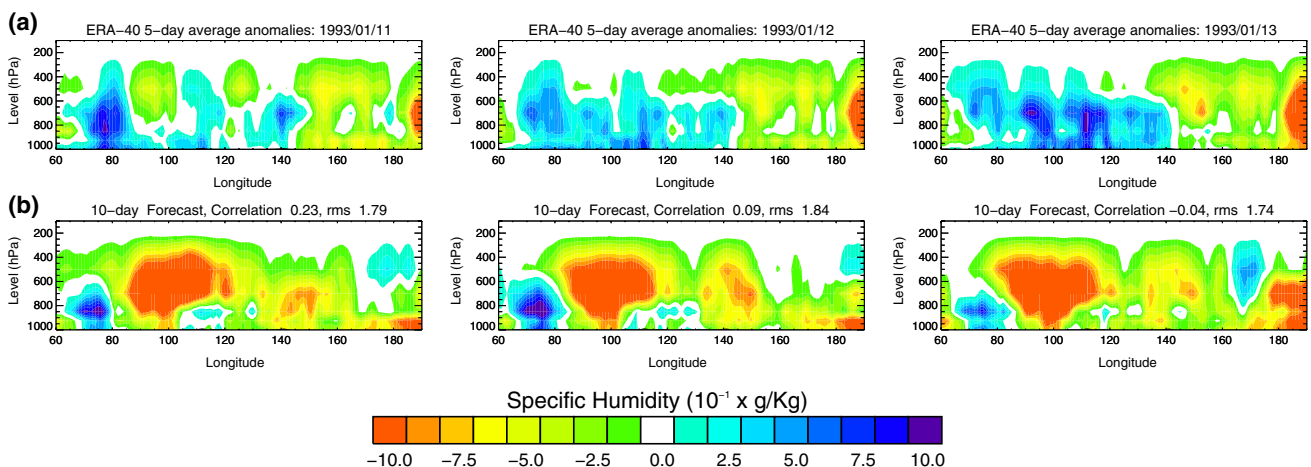


Fig. 4 Specific humidity in the Indo-West Pacific region (10°S – 10°N , 60°E – 170°W) for dates from January 11, 1993 to January 13, 1993. **a** Anomalies from ERA-40 data and **b** 10-day forecasts from control run

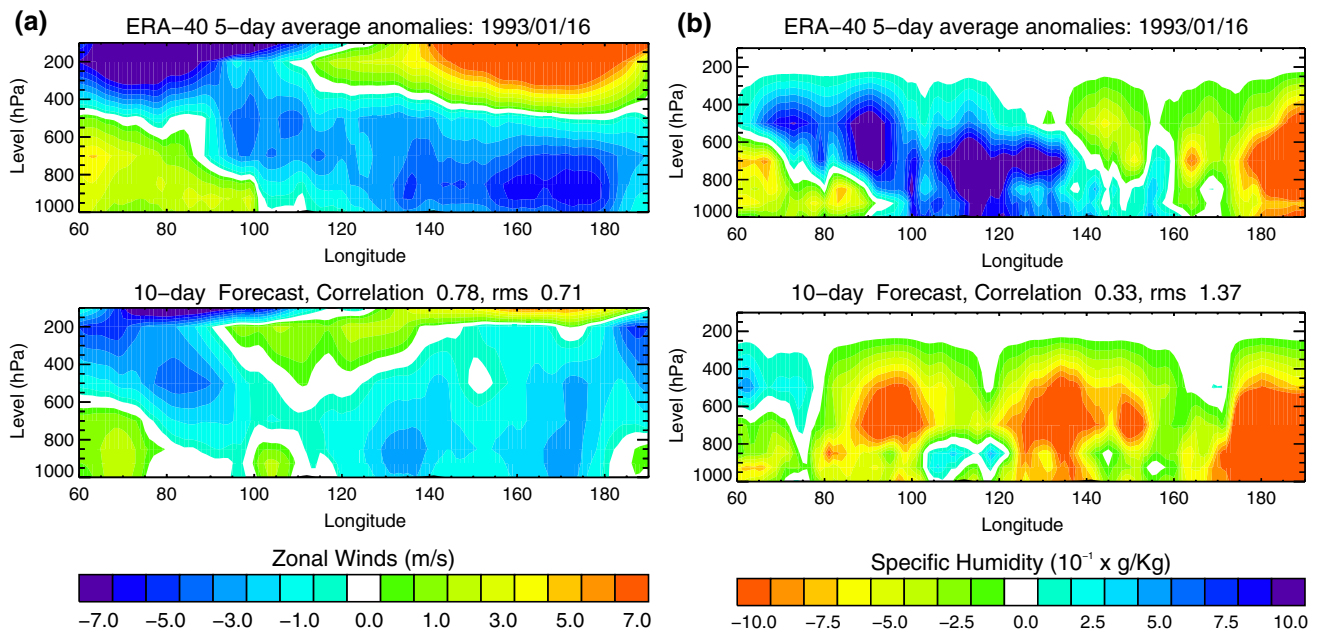


Fig. 5 ERA-40 anomalies and 10-day control forecast in the Indo-West Pacific region (10°S–10°N, 60°E–170°W) for January 16, 1993 of **a** zonal winds and **b** specific humidity

coincides well with ERA-40 in shape but not in magnitude (weak anomalies). Baroclinic structure is evident in both observations and 10-day forecasts, with low-level convergence and upper-level divergence. On the other hand, there is no skill in the specific humidity forecast for the same date and lead time (correlation 0.33, RMS error 1.37). The weak circulation anomalies in the forecasts are most likely a consequence of the relatively dry atmosphere. A drier atmosphere implies less latent heating in the atmospheric column, resulting in weaker circulation.

As can be seen in the bottom panels of Figs. 2 and 3, the overall forecast skill of the vertical structure of 5-day average zonal wind anomalies is considerably higher than that for specific humidity anomalies. In both cases the average correlation (standardized RMS error) decreases (increases) with forecast lead time, as expected. If we define a skillful forecast as one where the standardized RMS error is less than 1 (i.e. where the error in the forecast is less than the variability in the vertical structure in the selected region), then the forecasts for 5-day average anomalies of zonal winds in the equatorial Indian Ocean–West Pacific region associated with the ISO are skillful up to about 13 days. Using the same skill definition, the forecasts of specific humidity, which is associated with the moist convective anomalies during the ISO, have no skill whatsoever. It is important to note that this is a rather conservative definition of skill since at the point where the standardized RMS error is equal to 1, the forecasts are not useful for practical applications; the overall zonal wind forecasts (specific humidity) correlation is below the 99%

statistical significance threshold after a forecast lead time of 13 (8) days.

In order to estimate the forecast skill for the entire Indo-West Pacific basin, the model results were first interpolated to a 5-degree grid to avoid collocation errors. Area average temporal correlations, RMS, ensemble spread and ISO amplitude were estimated for every grid within the basin (30°S–30°N, 40°–180°E) for daily 200 and 850 hPa zonal winds and OLR and then spatially averaged to obtain a single value for the entire basin (Fig. 6). An important feature in the figure is the fact that the skill of the model forecasts, considering both correlation and RMS, is consistently better for 200 and 850 hPa zonal winds than for OLR, providing reasonably good forecasts during the first 11 (8) days for 200 hPa (850 hPa) zonal winds compared to about 4 days for OLR. Forecast skill for 850 hPa zonal winds is lower than for 200 hPa zonal winds. This difference in forecast skill is most likely due to boundary layer dynamics and thermodynamics (e.g. surface latent and sensible heat fluxes, boundary layer mixing, friction, low-level moisture convergence, etc.), which influence more directly the low-level circulation (850 hPa) than the upper troposphere (200 hPa).

If we use the ensemble spread as an indication of predictability (Fig. 6b), the time scale of predictability is considerably longer (~20–25 days) than the time scale of skillful forecasts for both variables. The gap between the ensemble spread and the RMS error can be regarded as unrealized predictability; in a perfect model both lines should overlap. Another possible explanation of the

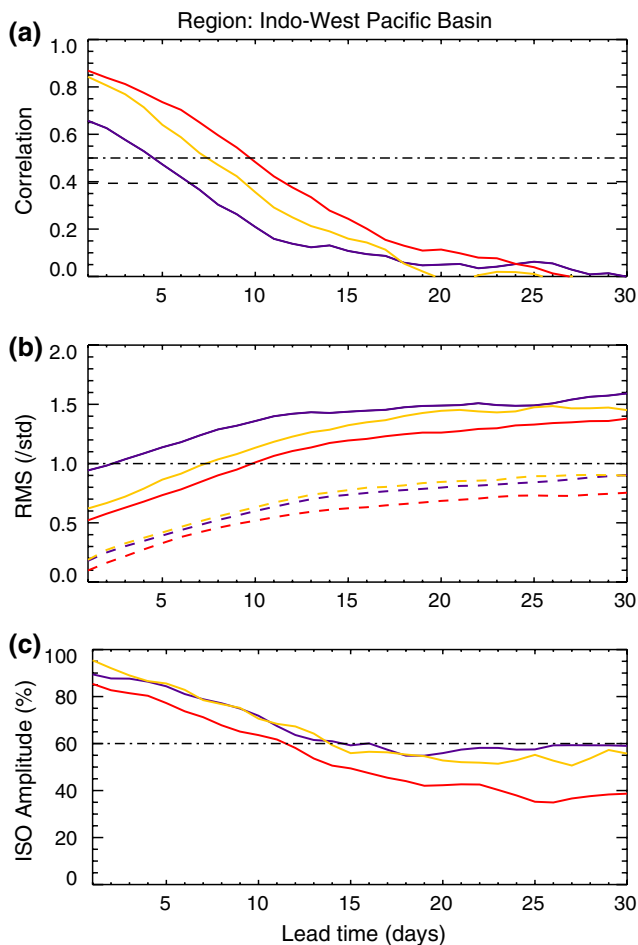


Fig. 6 Area average temporal **a** correlation, **b** standardized RMS and **c** relative intraseasonal amplitude over the Indo-West Pacific basin (30°S – 30°N , 40° – 180°E) for 200 hPa zonal winds (*red*) and OLR (*blue*). *Dotted lines* correspond to the average standardized ensemble spread (ensemble SD)

mismatch between ensemble spread and RMS is that the model is underestimating the uncertainties of the observed coupled system.

Figure 6c shows the basin-wide amplitude of the forecast ISO relative to the observations. The amplitude of the forecasts in the intraseasonal band does not represent by itself a measurement of the skill of the forecast. However, it provides additional information about the performance of the model. Due to the length of the forecasts (~ 30 days) the intraseasonal variability is obtained by first removing the linear trend in the forecasts and concurrent observations followed by a 10-day moving average of the detrended time series. Linear least squares regression was used to estimate the linear trends. The poor ISO forecast skill is not only evident in the phasing (correlation) and magnitude of the errors (RMS error), but also in the amplitude of the simulated intraseasonal variability. The model does not maintain the observed amplitude in the intraseasonal band.

The simulated amplitude is considerably lower than the observations, and decreases with the forecasting lead time. In other words, the ISO is damped or eroded by the model.

Analyses of the regional vertical structure of the forecasts indicate that weak circulation anomalies are produced by the model compared to those in ERA-40 and the model tends to simulate a dryer atmosphere. These two features are coherent since without the release of latent heating associated with deep convective events (positive anomalies of specific humidity) the circulation would tend to be weaker. Figure 7 shows the virtual potential temperature profiles from 1,000 to 500 hPa for a region in the Equatorial Indian Ocean (10°S – 10°N , 70 – 90°E) for December 22, 1992 from ERA-40 and the forecasts for the same date for different lead times (5, 10, 15, 20 and 25 days). Figure 7a shows the absolute values as well as the difference between 700 and 1,000 hPa virtual potential temperature, and Fig. 7b shows the deviation of the forecasts from the ERA-40 data. The profiles in Fig. 7a, b and the higher values of 700–1,000 hPa virtual potential temperature in the forecasts suggest a more stable atmosphere in the forecasts than the ERA-40 data. This behavior is observed throughout the entire period of the serial runs experiment as confirmed by the distribution of the differences between the forecast and observed 700–1,000 hPa virtual potential temperature for different lead times which shows that in most cases the 700–1,000 hPa virtual potential temperature is higher for the forecasts compared to ERA-40 data (i.e. higher likelihood of positive values in the distribution; Fig. 7c). The forecasts generate a more stable atmosphere compared to ERA-40 data, limiting the production of deep convective events associated with the ISO, as well as the moistening of the atmospheric column. The analysis shown in Fig. 7 was based on the control forecast; analysis of the four ensemble members shows similar results (figure not shown).

3.2 2002 and 2004 summer ISO cases

We now concentrate on the analysis of two ISO cases that took place during the boreal summers of 2002 and 2004 and compare the results with those obtained for the wintertime TOGA-COARE case. Both summer experiments correspond to intense intraseasonal convective anomalies propagating eastward towards the Pacific and northward into the Bay of Bengal and India, generating active and break periods of rainfall during the monsoon season. The first period evaluated starts April 15, 2002, which includes the growth of a large active period of the monsoon that year followed by an extended midseason break which cause an extensive drought in India. The second period begins May 18, 2004 and covers the growth of an active period associated with the Southeast Asian monsoon onset. For the

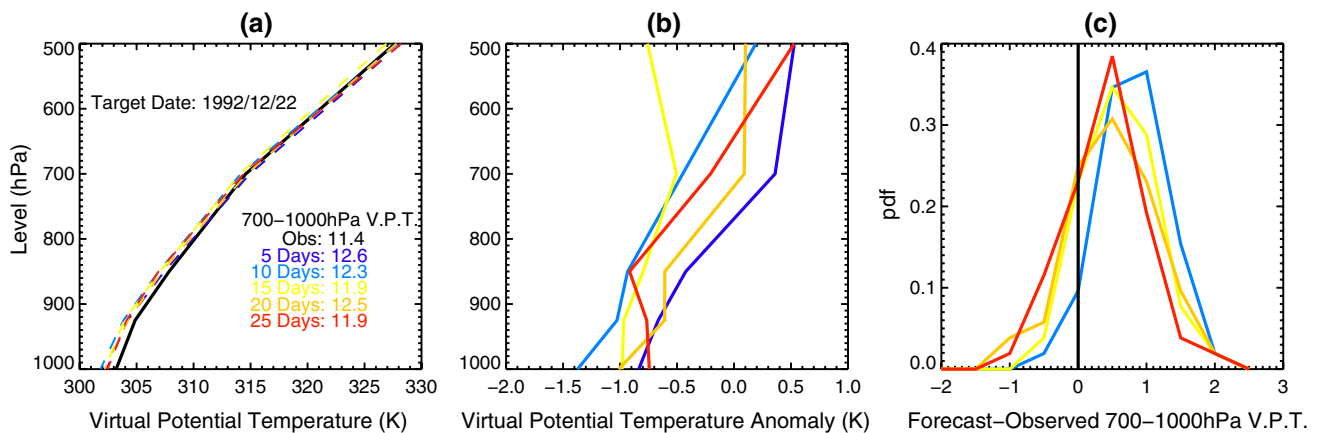


Fig. 7 Virtual potential temperature profiles in the Equatorial Indian Ocean (10°S – 10°N , 70 – 90°E) for December 22, 1992: **a** absolute values from ERA-40 and the forecasts for different lead times (5, 10, 15, 20 and 25 days) including the difference between 700 and 1000 hPa virtual potential temperature and **b** deviations of the

forecasts from ERA-40. **c** Distribution of the differences between the forecast and observed 700–1000 hPa virtual potential temperature for the entire TOGA-COARE serial run experiment and for different lead times

summer cases we include analysis of zonally average meridional wind anomalies in the longitudinal band between 70 and 90°E as well as the specific humidity anomalies in the same band to capture the northward propagation of convective anomalies.

Figures 8 and 9 show the distribution of correlation and standardized RMS error as a function of forecast lead time and time of forecast initiation for anomalies of zonal winds in the Indo-West Pacific region (similar to Fig. 2) for the 2002 and 2004 cases, respectively. The general results are similar for both cases and the TOGA-COARE case previously analyzed: the forecast amplitude of the 5-day average zonal circulation anomalies is smaller than those in the operational analysis; and the skill of the forecast decreases for convective episodes regardless of the starting date of the forecast (diagonal pattern in Figs. 8 and 9). However, the skill of the forecast improves when the low-level moistening is already present in the initial conditions, as was shown in Agudelo et al. (2006). Whether the errors around convective events are due to problems inherent to the convective parameterization, the flow-dependent nature of predictability in the coupled system, or a combination of both, is yet to be determined. However, these errors point to a fundamental weakness of the model in maintaining long-lived convective events (or convective clustering mechanisms in time) that is most likely translated into errors in the forecast circulation anomalies.

Analysis of the skill of 200 hPa zonal wind in the Equatorial Indian Ocean also suggests a concentration of errors around particular dates (Fig. 10). The figure shows the ensemble forecasts of 200 hPa zonal winds as well as the standard deviation of the ensemble members for all successive forecasts (starting day) and during the entire integration period (target day). The standard deviation is

computed relative to the observations (Fig. 10b) and to the ensemble mean (Fig. 10c). The first quantity provides information about the skill of the model and the latter is an indication of predictability. It is clear from Fig. 10a that the control model forecasts deviate considerably from observations. Figure 10b indicates that the forecasts deviate from observations particularly during periods of maximum ISO convective activity. The vertical orientation of these high error regions in the diagram indicates that no matter how close to the maximum ISO activity the model is initialized, the largest ensemble errors are always linked to this period. Figure 10c shows how the ensemble spread grows as the forecasting lead time increases. Notice that the magnitude of the internal ensemble spread is considerably smaller than the deviation from observations during ISO maxima, indicating low uncertainty of the model. The extremely different shapes of both standard deviation diagrams suggests that integration errors linked to the ISO are not arising due to small uncertainties in the initial conditions or in the model physics in a stochastic sense, but due to the model physics that result in biases during convective episodes. For a model with perfect physics, one would expect both diagrams to have a very similar structure. Evaluation of the 850 mb field gives similar results (not shown).

Analysis of the joint PDF between observations and forecasts allows a nonparametric examination of the structure of the forecasts at different percentiles, including the information from all ensemble members. The joint PDF (2D histogram) was estimated using all the observations and ensemble forecasts within the Indo-West Pacific basin (30°S – 30°N , 40° – 180°E) in a 5-degree spatial resolution. In other words, every observation-forecast pair for every ensemble and for every grid in the basin is included in the

Fig. 8 Same as Fig. 2 but for the 2002 summer case

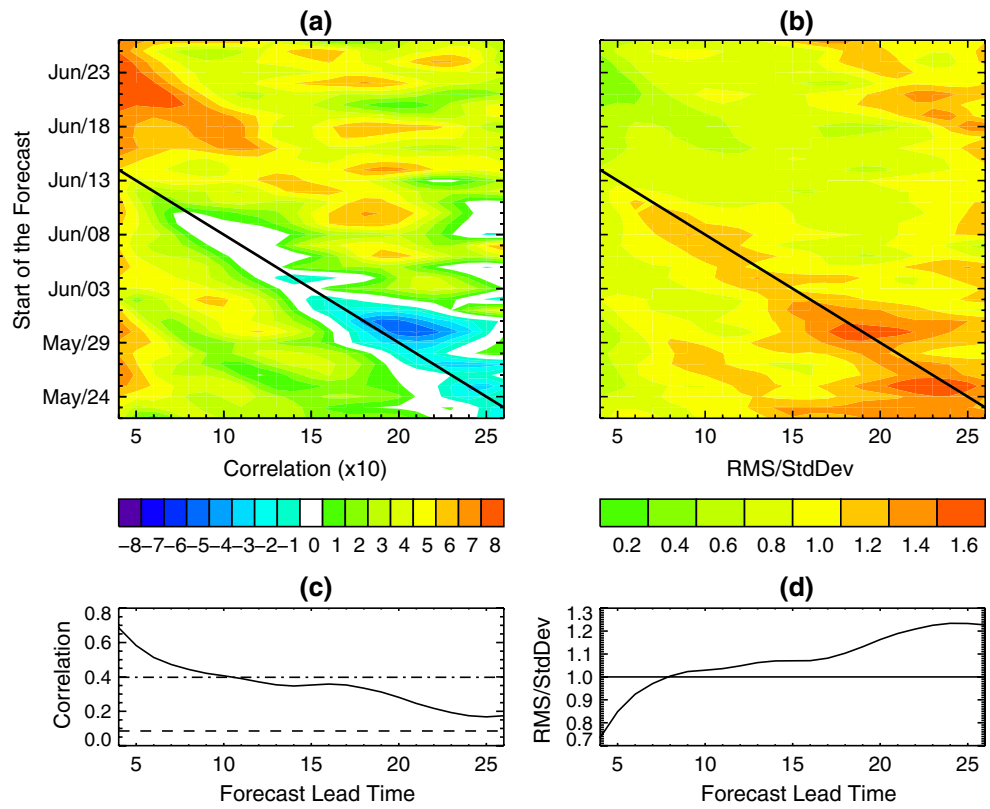
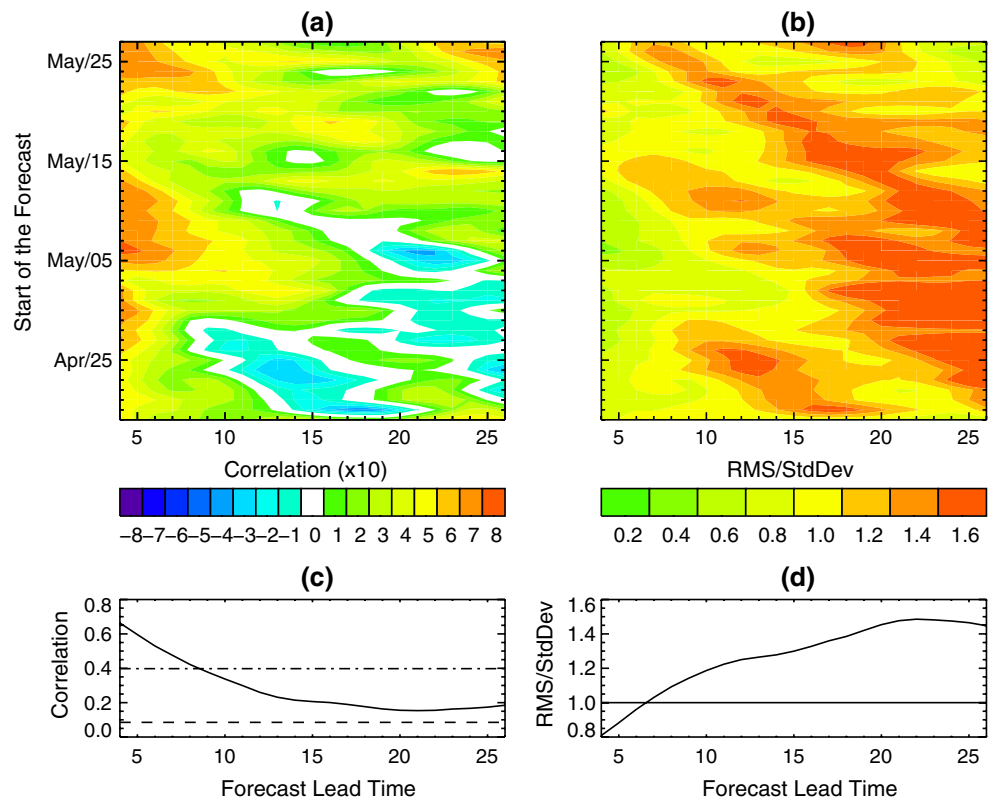


Fig. 9 Same as Fig. 2 but for the 2004 summer case



joint PDF. Figure 11 shows the joint PDF for different forecasting lead times (1, 8, 15 and 22 days) for 200 and 850 hPa zonal winds and OLR. There are two fundamental

differences between the sets of PDFs: (i) the OLR joint PDF shows considerably greater spread around the perfect forecast line (higher error) than the zonal wind PDFs, and

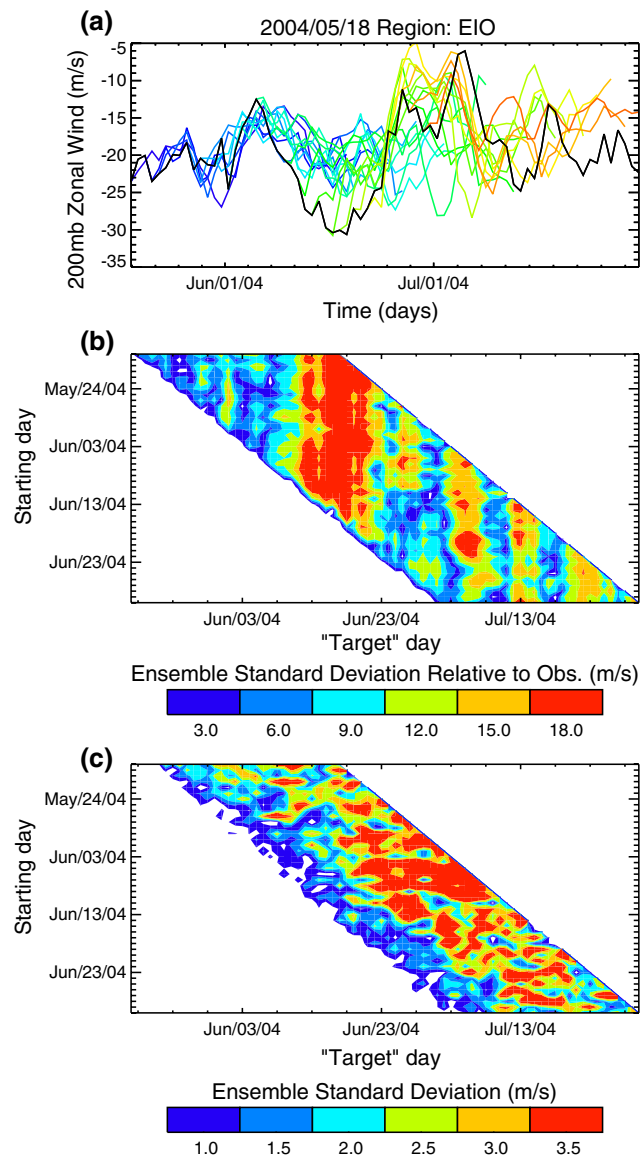


Fig. 10 a 30-day evolution of the 200 hPa zonal winds ensemble mean in the Equatorial Indian Ocean (10°S–10°N, 70–90°E) for the 2004 experiment (colored lines) as well as the observations (black line), and the standard deviation of the ensemble members for all the successive forecasts computed relative to b the observations and c the ensemble mean

more importantly, (ii) while the errors in zonal winds are distributed uniformly in the entire range of observed winds the errors in OLR are far from uniform, with considerably higher errors for low values of OLR which in the tropics are generally associated of convective clouds. Using the joint PDF, it is possible to estimate different non-parametric skill measurements such as the forecast success rate in different intervals. Figure 11 shows the success rate in four non-overlapping equal-area regions. The areas are defined as one quarter of the variable range (from minimum to maximum) by one standard deviation of the

observations ($\pm 1/2$ standard deviation). In this context, a forecast is regarded as successful if both the observation and the forecast fall in the same area. The success rate is then defined for each area as the ratio between the number of successful forecasts and sum of successes and failures. It is clear that the success rate of OLR depends strongly on the actual magnitude of OLR to be forecast, suggesting that the model simulates the suppressed conditions better than transitional and convectively active conditions, supporting the findings of Agudelo et al. (2006). For zonal winds, there is a difference in the success rate relative to the area, but not as strong as for OLR.

The time horizon for skillful forecasts (where standardized RMS < 1) during summer is between 5 and 7 days (Figs. 8 and 9), while during winter the time horizon for skillful forecasts is at least twice as long. Analysis of the vertical structure of meridional wind anomalies over the Indian monsoon region (10°S–35°N, 75–95°E) during summer also shows an average time horizon of skillful forecasts around 7 days (Fig. 12a, b). While the analysis only includes serial experiments for three ISO events, it suggests that the skill of the forecast is greater for winter ISO cases than for summer events. This result is most likely due to the fact that the circulation structure of the summer ISO is more complex, as it has not only an eastward propagating branch but also a northward propagating one. Since the results for both summer cases are similar, henceforth only results for the 2004 case will be presented.

The zonal vertical structure around the equator during summer shows very similar results to those found during winter, with significantly lower forecast skill for specific humidity than for zonal and meridional wind and with the model predicting a drier atmosphere than the operational analysis. However, analysis of the meridional vertical structure of specific humidity anomalies presents an interesting and counterintuitive feature. In Fig. 12c and d, both the increasing correlation and the decaying RMS for forecast lead times greater than 8 days would suggest that the extended-range forecasts become more skillful as the forecast horizon increases. Since this is not likely, understanding what is causing this result points to a critical aspect of the model.

Figure 13 shows the 5-day average specific humidity anomalies in the Indian monsoon region for four different dates from operational analysis and for 10-day forecasts of the same dates. The four operational analysis panels (Fig. 13a, b, e, f) show the evolution of a typical summer ISO event. Specifically, in Fig. 13a, the anomalies show the start of an active phase around the equator and predominantly suppressed conditions over the continent. During the transition stage (Fig. 13b), convection commences over the continent. In Fig. 13e, f convective anomalies have already moved northward completely and

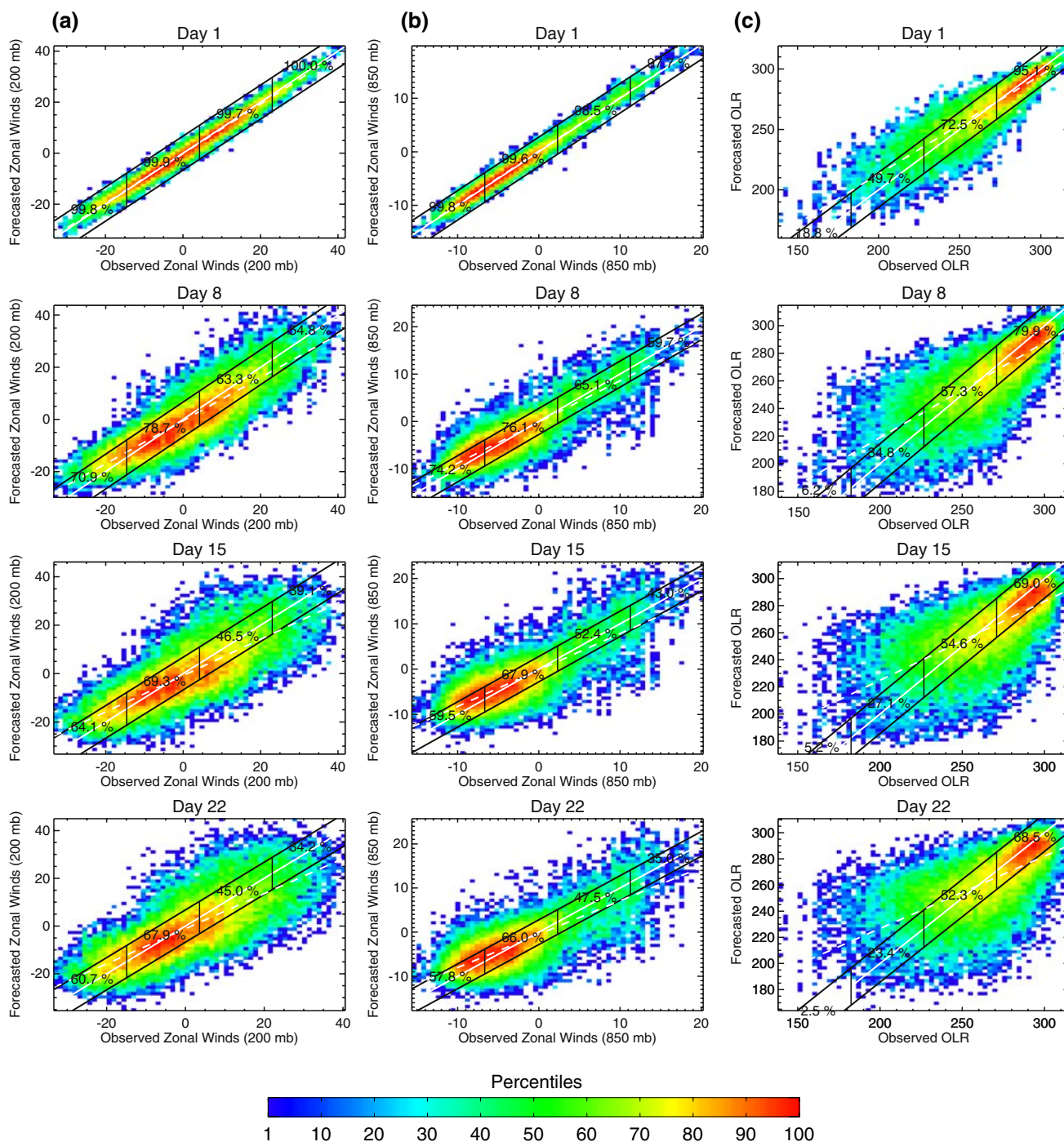


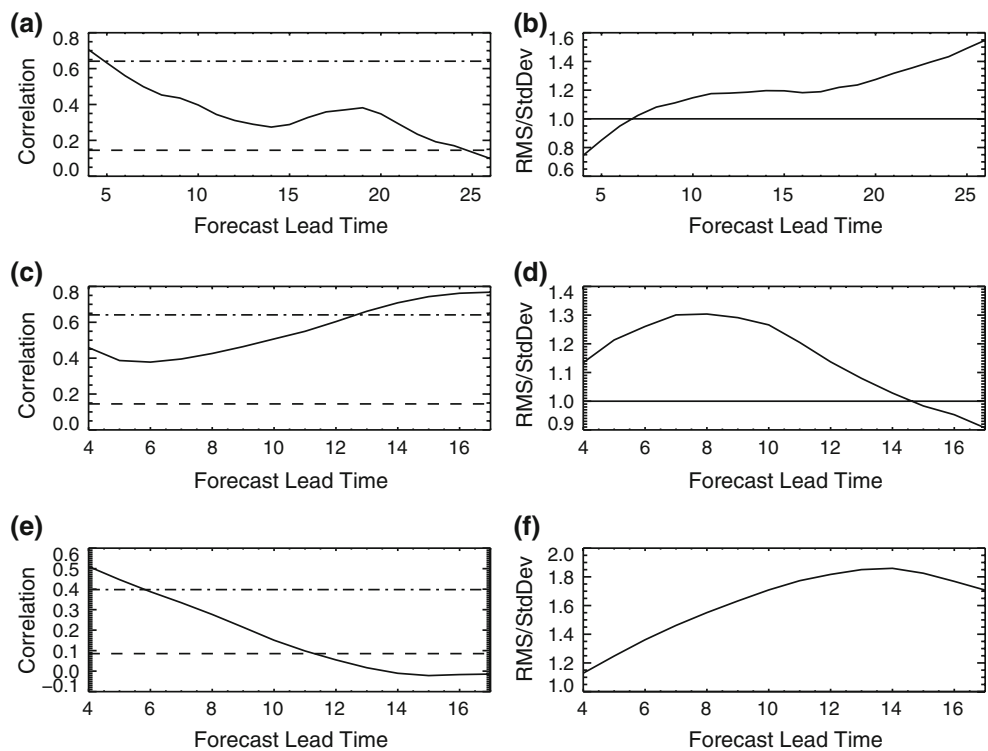
Fig. 11 Joint probability density function between observed and forecast **a** 200 hPa and **b** 850 hPa zonal winds (m s^{-1}) and **c** OLR (W m^{-2}) for different lead times (1, 8, 15 and 22) over the Indo-West Pacific basin (30°S – 30°N , 40° – 180°E). The probability density

increases from *blue* to *red*. The *white* continuous line corresponds to perfect forecasting and the *dashed* line to the actual linear fit between forecasts and observations. The *black* lines correspond to half standard deviation of the observations

suppressed conditions dominate the equatorial region. The diagrams also show evidence of the weaker convective branch that propagates southward. The skill of the 10-day forecast is higher when convection is occurring over India. Active and suppressed convection over the continent during summer are controlled by the propagation of positive

and negative intraseasonal anomalies that originate over the equatorial Indian Ocean. Since the model is not able to forecast skillfully the generation of specific humidity anomalies in the Indian Ocean around the equator as shown in the analysis of zonal vertical structure, convective anomalies would not propagate from the equator. This

Fig. 12 Average **a** correlation and **b** RMS error for meridional wind anomalies over the Indian monsoon region (10°S–35°N, 75–95°E) for each forecast lead time; **c** and **d** same as **a** and **b** but for meridional specific humidity, **e** and **f** same as **a** and **b** but for zonal specific humidity



means that other mechanisms different to the ISO are modulating the model rainfall over the South-East Asian continent in the model: what is shown in the 10-day forecasts in Fig. 13 is evidence of the annual character of the monsoon and not of intraseasonal variability. In other words, the model forecasts are reproducing reasonably well the annual structure of the monsoon with significant rainfall north of 15°N. Since the model does not reproduce the suppressed and active sequence over the continent, the result is a meridionally-permanent active-like phase in the forecasts. Given that the model is always forecasting an active-like phase of the monsoon, the model will match the observations when actual active conditions are present over India, artificially increasing the skill in some phases. The fact that only the skill for meridional humidity anomalies increases with forecast lead time (Fig. 12c and d) while it decreases for meridional winds in the 70–90°E band (Fig. 12a and b) as well as for zonal winds (Fig. 9) and humidity around the equator (Fig. 12e and f) is a further indication of the artificial increase in skill influenced by biases in the monsoon annual cycle.

In the analysis of the wintertime TOGA-COARE case, it was pointed out that the atmosphere around the equatorial Indian Ocean warm pool was drier than the ERA-40 during ISO events. It is important to note that the model is not drier than the ERA-40 everywhere. Specifically, during summer the forecast humidity anomalies relative to observations suggest a wetter atmosphere over the South-East Asian continent compared to observations. However,

the origin of these anomalies is very different: in the winter case the dryer atmosphere in the intraseasonal band is due to the lack of model skill to develop and sustain a long-lived convective envelope. During summer, the overall anomalies over land are associated with biases in the forecast annual cycle relative to the operational analysis.

A range of evidence has been presented suggesting that the model's skill is lower for periods associated with convection both during winter and summer. Figure 14 shows the spatial distribution of the standardized RMS errors of 200 mb zonal winds for the summer 2004 experiment for the first 8 days of the forecast. The spatial distribution of the errors in the forecasts for days 1 and 2 are remarkably similar in both cases to the cumulative precipitation distribution during the duration of the experiment. Results are similar for the 2002 summer case as well as for the wintertime TOGA-COARE case. Similar features are also observed when analyzing the spatial distribution of errors for 850 hPa zonal winds. The main differences are over land, where topography and terrestrial boundary layer dynamics affects the 850 hPa zonal winds, resulting in larger errors over land that are not evident for the 200 hPa winds. After day 1 and 2, errors emanate from the convective regions, covering the entire tropics, dampening or eroding the development of an intraseasonal oscillation and potentially modulating the extended-range forecast skill of extratropical weather.

Figure 15 shows scatter plots of the observed (i.e. operational analysis) 2 m temperature and the observed

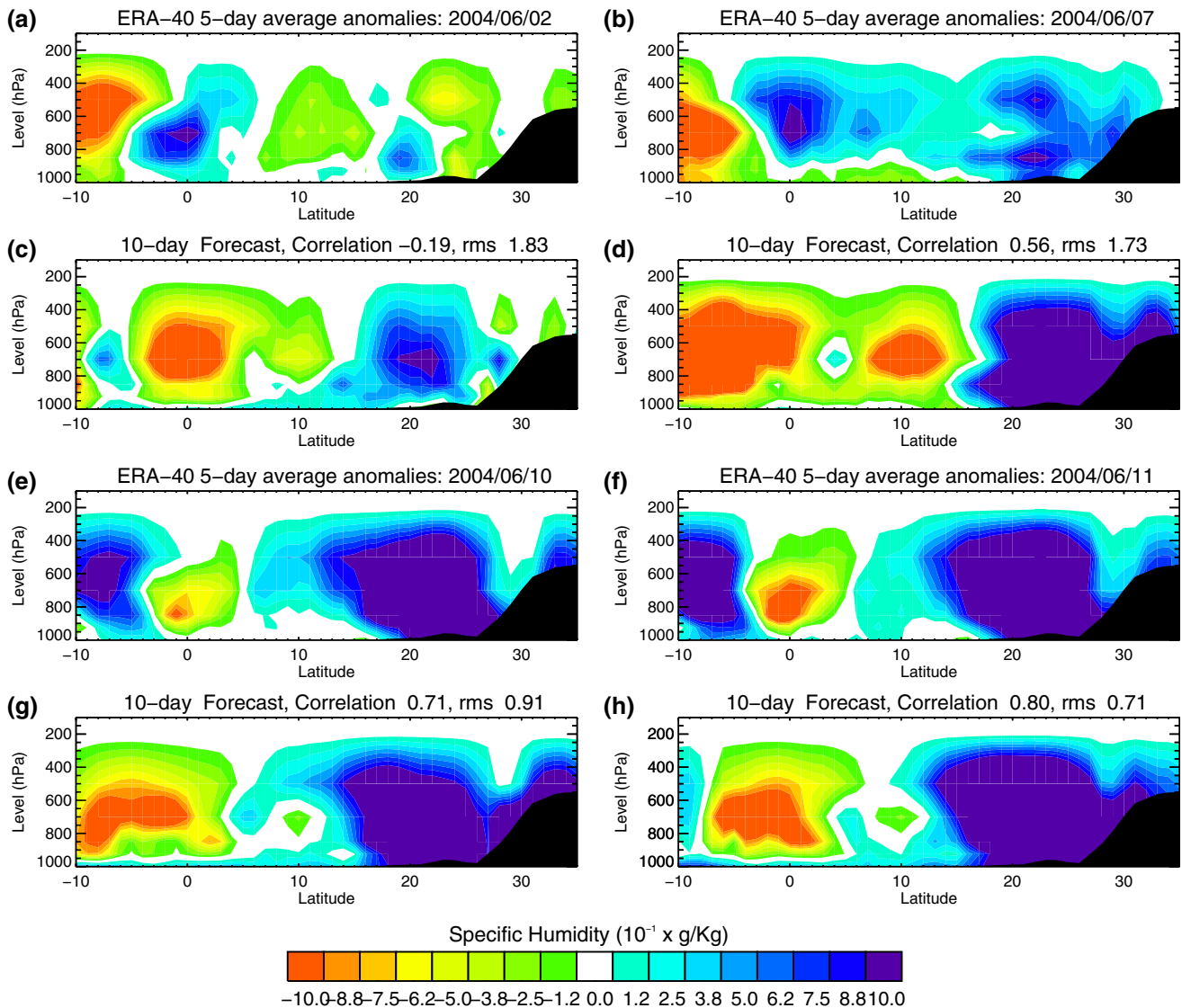


Fig. 13 5-day average specific humidity anomalies over the Indian monsoon region (10°S–35°N, 75–95°E) for four different dates from the ECMWF operational analysis (a, b, e, f) and for 10-day forecasts (c, d, g, h)

boundary layer height in the Equatorial Indian Ocean as well as the forecast boundary layer heights in the summer 2004 experiment. The goal of this diagram is to evaluate the skill of the model using a signature relationship that summarizes the role of air–sea interaction (i.e. boundary layer processes) in the deep convection. Observed 2 m temperature was used as the independent variable in the figure instead of time given the strong relationship between this variable and the boundary layer height (Fig. 15a), where a deep boundary layer is associated with high 2 m temperature and vice versa, evidencing the strong air–sea interaction in the region given the strong association between SST and 2-m temperature. In this manner, such relationship serves as a direct benchmark for the model forecasts: in order for the model to be able to forecast

accurately the near-surface processes, it should be able to reproduce, in shape and magnitude, the observed relationship between both variables. The variability of boundary layer height is important for the ISO life cycle given that the boundary layer contains a large percent of the total atmospheric moisture, thus determining to a large degree the amount of energy available to fuel deep convection. Contrary to the observations, it can be seen from the Fig. 15 that the relationship between 2 m temperature and boundary layer height disappears quickly as the lead time increases. In addition, the model tends to generate a 20% shallower boundary layer compared to the operational analysis. These findings suggest that the errors in the boundary layer height, which is the collective outcome of all different low-level processes including surface friction,

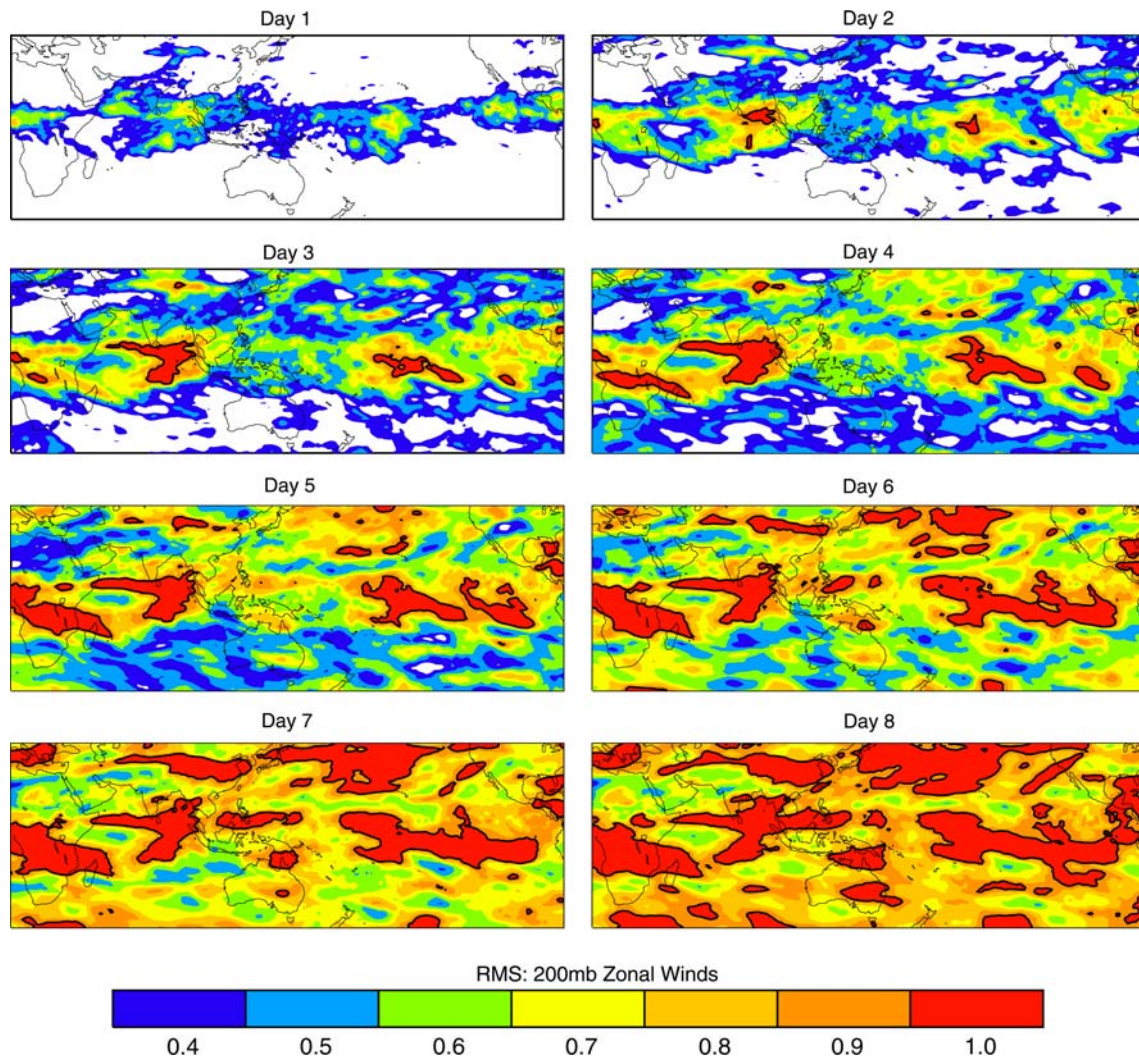


Fig. 14 Spatial distribution of the 200 hPa zonal winds standardized RMS error for the summer 2004 experiment for different forecast lead times

ocean–atmosphere heat exchanges, and low-level moisture convergence, are associated with the poor timing and magnitude of the positive humidity anomalies and deep convection in the model as shown in Figs. 3, 9, 11. In addition, the model forecasts underestimate the magnitude of surface latent heat flux by about $20\text{--}40\text{ W m}^{-2}$ (Agudelo et al. 2006), contributing to the errors in the humidity in the model forecasts.

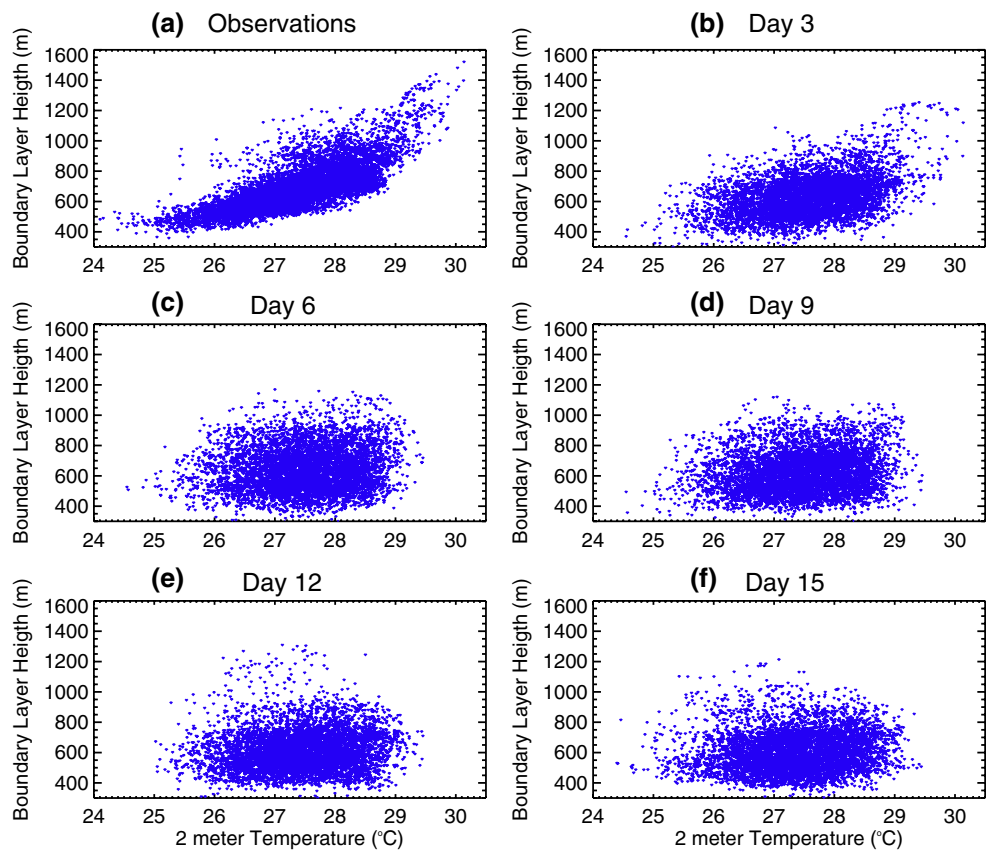
4 Discussion and conclusions

The extended-range forecast skill of the ECWMF operational forecast model was evaluated in the framework of a serial runs experiment in the presence of ISO events during winter (TOGA-COARE) and summer (2002 and 2004) cases. This framework allows an accurate estimation of the forecast skill throughout the entire life cycle of selected

ISO events and identification of the origin of errors in the forecast. Distinguishing features of this analysis relative to previous studies include: analysis of both wintertime and summertime ISOs; analysis method of serial forecasts to focus on identifying the origin of model errors; and examination of the entire vertical structure of circulation and humidity anomalies in the intraseasonal band as well as the horizontal 2D fields.

Correlation and standardized RMS error analysis of the vertical structure of ISO anomalies suggests that the useful forecast time scale for circulation anomalies (zonal winds) is about 13 days during winter compared to about 7–8 days during summer. However, the forecast skill is not stationary and presents evidence of a flow-dependent nature: not only is the forecast skill a function of initial conditions but also, and more importantly, there are states of the coupled system, corresponding to long-lived convective envelopes associated with the ISO, for which forecast skill is always

Fig. 15 Scatter plots of observed 2 m temperature versus the **a** observed boundary layer height and versus **b–f** the forecast boundary layer height for different lead times for the summer 2004 experiment. The region considered in the analysis corresponds to the Equatorial Indian Ocean (10 °S–10°N, 70–90°E)



low regardless of the starting date of the forecast. These results are consistent with previous research (e.g. Hendon et al. 2000). Whether the errors associated with convective events are due to problems inherent to the convective parameterization or due to an intrinsic lack of predictability in the coupled system associated with moist convection, is yet to be determined. However, the spread between the 5 ensemble members was found to be limited (small compared to RMS estimations), suggesting that the model underestimates the uncertainties of the coupled system even considering that the tendencies of the atmospheric physics are randomly perturbed throughout the integrations. While the set of ensembles is small, this indicates that problems with atmospheric physics, and especially with convective and boundary layer parameterizations, are the likely cause of the flow-dependent nature exhibited by the forecast skill.

Even though the number of ISO cases evaluated in this study is limited (although not the number of independent simulations), results suggest a considerably better forecast skill during the winter ISO than for summer events. Von Storch and Xu (1990) found a similar result using a statistical forecasting scheme of an MJO index. A possible explanation for the seasonal difference in the forecasts is that the circulation structure of the summer ISO is more complex than during winter, with a northward propagating

convective center as well as an eastward propagating one. Results for the summer case suggest that models nearly always forecast an active-like phase of the South-east Asian summer Monsoon. This active-like phase is consistent with biases in the annual character of the monsoon. The spatial structure of the annual cycle of the monsoon is similar to that of a suppressed phase over the equatorial Indian Ocean during summer: dry near the equator and wet over Southeast Asia. Relative to observations, anomalies of a strong (weak) monsoon appear as a break (active) phase over the equator. We argue that one of the reasons for the existence of model biases in the monsoon system is the lack of a strong ISO in the extended-range forecasts, and further northward propagation of dry and wet anomalies towards the Southeast Asian continent. Without such propagation of the anomalies, the monsoon lacks intraseasonal modulation over the continent hence the annual cycle prevails during the entire season, altering the seasonal cumulative rainfall. Analysis of observations suggests that the cumulative effect of intraseasonal oscillations introduces internal interannual variability of the monsoon system (Hoyos and Webster 2007). Further research is needed to establish the cause of lack of northward propagation in the model. It appears that not only the convective parameterization but also the representation of boundary layer processes might explain this absence.

Consistent with previous studies (e.g. Waliser et al. 2003), the forecast skill of circulation-associated anomalies is far better than that of moist convective anomalies. In general, the model lacks skill to simulate the long-lived moist convective envelope associated with the ISO. Humidity and circulation anomalies in the forecasts are very small compared to those in ERA-40. One possible explanation for the weak anomalies is that the model tends to generate a more stable atmosphere, thus limiting the model's capability to reproduce deep convective events associated with the ISO. Generating an atmosphere that is too stable relative to observations inhibits the build-up of convective available potential energy (CAPE). One of the consequences of the lack of CAPE and the poor representation of the convective events is that the amplitude of the ISO in the models quickly goes to zero as the integration time increases. Further research is needed to understand why the model produces a more stable atmosphere, focusing on studying processes such as boundary layer dynamics and surface heat fluxes, low-level moisture convergence, convective parameterizations and triggering functions of convection.

The analysis presented here implies that the representation of the convective processes is in the heart of the lack of extended forecast skill. Not only is the forecast skill of moist convection less than that of circulation anomalies, but evidence suggests that the representation of convection in the model is associated with the dampening or erosion of the ISO anomalies in the model forecasts.

Acknowledgments This research has been supported by the National Science Foundation's Atmospheric Science Division under NSF Grant ATM-0531771 (PJW) and by National Oceanic and Atmospheric Administration's Climate Prediction Program for America under NOAA grant GCO6-196 (PJW). ECMWF ERA-40 data used in this study was obtained from the ECMWF data server. We would particularly like to acknowledge Frederic Vitart, Tim Palmer and Martin Miller for making the serial integrations of the ECMWF model available for analysis.

References

- Agudelo PA, Curry JA, Hoyos CD, Webster PJ (2006) Transition between suppressed and active phases of intraseasonal oscillations in the Indo-Pacific warm pool. *J Clim* 19:5519–5530. doi:10.1175/JCLI3924.1
- Balmaseda MA, Anderson DLT, Vidard A (2005) Ocean analysis at ECMWF: from real time ocean initial conditions to historical reanalysis. *ECMWF Newsl* 105:24–32
- Buizza R, Miller M, Palmer TN (1999) Stochastic representation of model uncertainties in the ECMWF ensemble prediction system. *Q J R Meteorol Soc* 125:2887–2908. doi:10.1256/smsqj.56005
- Buizza R, Palmer TN (1995) The singular-vector structure of the atmospheric global circulation. *J Atmos Sci* 52:1434–1456. doi:10.1175/1520-0469(1995)052<1434:TSVSOT>2.0.CO;2
- Chen TC, Alpert JC (1990) Systematic errors in the annual and intraseasonal variations of the planetary-scale divergent circulation in NMC medium-range forecasts. *Mon Weather Rev* 118:2607–2623. doi:10.1175/1520-0493(1990)118<2607:SEITAA>2.0.CO;2
- Drbohlav HKL, Wang B (2007) Horizontal and vertical structures of the northward-propagating intraseasonal oscillation in the South Asian monsoon region simulated by an intermediate model. *J Clim* 20:4278–4286. doi:10.1175/JCLI4244.1
- Ferranti L, Palmer TN, Molteni F, Klinker E (1990) Tropical-extratropical interaction associated with the 30–60-day oscillation and its impact on medium and extended range prediction. *J Atmos Sci* 47:2177–2199. doi:10.1175/1520-0469(1990)047<2177:TEIAWT>2.0.CO;2
- Fu X, Wang B (2004) Differences of boreal summer intraseasonal oscillations simulated in an atmosphere–ocean coupled model and an atmosphere-only model. *J Clim* 17:1263–1271. doi:10.1175/1520-0442(2004)017<1263:DOBSIO>2.0.CO;2
- Fu X, Wang B, Li T, McCreary JP (2003) Coupling between northward propagation intraseasonal oscillations and sea surface temperature in the Indian Ocean. *J Atmos Sci* 60:1733–1753. doi:10.1175/1520-0469(2003)060<1733:CBNIOA>2.0.CO;2
- Gustafson WI, Weare BC (2004) MM5 modeling of the Madden-Julian oscillation in the Indian and West Pacific Oceans: model description and control run results. *J Clim* 17:1320–1337. doi:10.1175/1520-0442(2004)017<1320:MMOTMO>2.0.CO;2
- Hendon HH, Liebmann B (1990) The intraseasonal (30–50 day) oscillation of the Australian summer monsoon. *J Atmos Sci* 47:2909–2924. doi:10.1175/1520-0469(1990)047<2909:TIDOOT>2.0.CO;2
- Hendon HH, Salby ML (1994) The life cycle of the Madden-Julian oscillation. *J Atmos Sci* 51:2207–2219. doi:10.1175/1520-0469(1994)051<2225:TLCOTM>2.0.CO;2
- Hendon HH, Liebmann B, Newman M, Glick J (2000) Medium-range forecast errors associated with active episodes of the Madden-Julian oscillation. *Mon Weather Rev* 128:69–86. doi:10.1175/1520-0493(2000)128<0069:MRFEAW>2.0.CO;2
- Hoyos CD, Webster PJ (2007) The role of intraseasonal variability in the nature of asian monsoon precipitation. *J Clim* 20:4402–4424. doi:10.1175/JCLI4252.1
- Inness PM, Slingo JM, Guilyardi E, Cole J (2003) Simulation of the Madden-Julian oscillation in a coupled general circulation model. Part II: The role of basic state. *J Clim* 16:345–364. doi:10.1175/1520-0442(2003)016<0345:SOTMJO>2.0.CO;2
- Jones C, Waliser DE, Schemm JKE, Lau WKM (2000) Prediction skill of the Madden-Julian oscillation in dynamical extended range forecasts. *Clim Dyn* 16:273–289. doi:10.1007/s003820050327
- Kemball-Cook SR, Weare BC (2001) The onset of convection in the Madden-Julian oscillation. *J Clim* 14:780–793. doi:10.1175/1520-0442(2001)014<0780:TOOCIT>2.0.CO;2
- Kiladis GN, Straub KH, Haertel PT (2005) Zonal and vertical structure of the Madden-Julian oscillation. *J Atmos Sci* 62:2790–2809. doi:10.1175/JAS3520.1
- Kim H-M, Hoyos CD, Webster PJ, Kang I-S (2008) Sensitivity of MJO simulation and predictability to sea surface temperature variability. *J Clim* (in press). doi:10.1175/2008JCLI2078.1
- Lau K-M, Waliser DE (2005) Intraseasonal variability of the atmosphere–ocean climate system. Springer Heidelberg, Germany, p 474
- Lau KM, Chang FC (1992) Tropical intraseasonal oscillation and its prediction by the NMC operational model. *J Clim* 5:1365–1378. doi:10.1175/1520-0442(1992)005<1365:TIOAIP>2.0.CO;2
- Lawrence D, Webster PJ (2002) The boreal summer intraseasonal oscillation and the South Asian monsoon. *J Atmos Sci* 59:1593–1606. doi:10.1175/1520-0469(2002)059<1593:TBSIOR>2.0.CO;2
- Lin JL, Kiladis GN, Mapes BE, Weickmann KM, Sperber KR, Lin WY et al (2006) Tropical intraseasonal variability in 14 IPCC

- AR4 climate models. Part I: convective signals. *J Clim* 19:2665–2690. doi:[10.1175/JCLI3735.1](https://doi.org/10.1175/JCLI3735.1)
- Lin X, Johnson RH (1996) kinematic and thermodynamic characteristics of the flow over the western Pacific warm pool during TOGA-COARE. *J Atmos Sci* 53:695–715. doi:[10.1175/1520-0469\(1996\)053<0695:KATCOT>2.0.CO;2](https://doi.org/10.1175/1520-0469(1996)053<0695:KATCOT>2.0.CO;2)
- Madden RA (1986) Seasonal variations of the 40–50 day oscillation in the tropics. *J Atmos Sci* 43:3138–3158. doi:[10.1175/1520-0469\(1986\)043<3138:SVOTDO>2.0.CO;2](https://doi.org/10.1175/1520-0469(1986)043<3138:SVOTDO>2.0.CO;2)
- Madden RA, Julian PR (1994) Observations of the 40–50 day tropical oscillation: a review. *Mon Weather Rev* 122:813–837. doi:[10.1175/1520-0493\(1994\)122<0814:OOTDIO>2.0.CO;2](https://doi.org/10.1175/1520-0493(1994)122<0814:OOTDIO>2.0.CO;2)
- Maloney ED, Hartmann DL (2000) Modulation of eastern North Pacific hurricanes by the Madden–Julian oscillation. *J Clim* 13:1451–1460. doi:[10.1175/1520-0442\(2000\)013<1451:MOENPH>2.0.CO;2](https://doi.org/10.1175/1520-0442(2000)013<1451:MOENPH>2.0.CO;2)
- Palmer TN, Shutts GJ, Hagedorn R, Doblas-Reyes FJ, Jung T, Leutbecher M (2005) Representing model uncertainty in weather and climate prediction. *Annu Rev Earth Planet Sci* 33:163–193. doi:[10.1146/annurev.earth.33.092203.122552](https://doi.org/10.1146/annurev.earth.33.092203.122552)
- Puri K, Barkmeijer J, Palmer TN (2001) Tropical singular vectors computed with linearized diabatic physics. *Q J R Meteorol Soc* 127:709–731. doi:[10.1002/qj.49712757222](https://doi.org/10.1002/qj.49712757222)
- Reynolds C, Webster PJ, Kalnay E (1994) Random error growth in the numerical prediction models. *Mon Weather Rev* 122:1281–1305. doi:[10.1175/1520-0493\(1994\)122<1281:REGING>2.0.CO;2](https://doi.org/10.1175/1520-0493(1994)122<1281:REGING>2.0.CO;2)
- Sheng JA (1995) The Madden–Julian oscillation in the Canadian climate center general circulation model. *Clim Dyn* 12:125–140. doi:[10.1007/BF00223725](https://doi.org/10.1007/BF00223725)
- Slingo JM et al (1996) Intraseasonal oscillations in 15 atmospheric general circulation models: results from an AMIP diagnostic subproject. *Clim Dyn* 12:325–357 doi:[10.1007/BF00231106](https://doi.org/10.1007/BF00231106)
- Simmons AJ, Gibson JK (2000) The ERA-40 project plan, ERA-40 Proj. Rep Ser ECMWF, Reading, UK 1: 62
- Sperber KR (2003) Propagation and the vertical structure of the Madden–Julian oscillation. *Mon Weather Rev* 131:3018–3037. doi:[10.1175/1520-0493\(2003\)131<3018:PATVSO>2.0.CO;2](https://doi.org/10.1175/1520-0493(2003)131<3018:PATVSO>2.0.CO;2)
- Stephens GL, Webster PJ, Johnson RH, Engelen R, L’Ecuyer T (2004) Observational evidence for the mutual regulation of the tropical hydrological cycle and tropical sea surface temperatures. *J Clim* 17:2213–2224. doi:[10.1175/1520-0442\(2004\)017<2213:OEFTMR>2.0.CO;2](https://doi.org/10.1175/1520-0442(2004)017<2213:OEFTMR>2.0.CO;2)
- Tracton MS, Mo K, Chen W, Kalnay E, Kistler R, White G (1989) Dynamical extended-range forecasting (DERF) at the National Meteorological Service. *Mon Weather Rev* 117:1604–1635. doi:[10.1175/1520-0493\(1989\)117<1604:DERFAT>2.0.CO;2](https://doi.org/10.1175/1520-0493(1989)117<1604:DERFAT>2.0.CO;2)
- Terray L, Sevault E, Guilyardi E, Thual O (1995) OASIS 2.0, user’s guide and reference manual. Technical report
- Tian BJ, Waliser DE, Fetzer E, Lambrigtsen B, Yung Y, Wang B (2006) Vertical moist thermodynamic structure and spatial–temporal evolution of the Madden–Julian oscillation in atmospheric infrared sounder observations. *J Atmos Sci* 63:2462–2485. doi:[10.1175/JAS3782.1](https://doi.org/10.1175/JAS3782.1)
- Uppala SM et al (2005) The ERA-40 re-analysis. *Q J R Meteorol Soc* 131:2961–3012 doi:[10.1256/qj.04.176](https://doi.org/10.1256/qj.04.176)
- Vialard J, Vitart F, Balmaseda MA, Stockdale T, Anderson DLT (2003) An ensemble generation method for seasonal forecasting with an ocean–atmosphere coupled model. *Mon Weather Rev* 133:441–453. doi:[10.1175/MWR-2863.1](https://doi.org/10.1175/MWR-2863.1)
- Vitart F (2004) Monthly forecasting at ECMWF. *Mon Weather Rev* 132:2761–2779. doi:[10.1175/MWR2826.1](https://doi.org/10.1175/MWR2826.1)
- Vitart F, Woolnough S, Balmaseda MA, Tompkins AM (2007) Monthly forecast of the Madden–Julian oscillation using a coupled GCM. *Mon Weather Rev* 135:2700–2715. doi:[10.1175/MWR3415.1](https://doi.org/10.1175/MWR3415.1)
- Von Storch H, Xu J (1990) Principal oscillation pattern analysis of the tropical 30–60 day oscillation. Part I: definition of an index and its prediction. *Clim Dyn* 4:179–190. doi:[10.1007/BF00209520](https://doi.org/10.1007/BF00209520)
- Waliser DE, Jones C, Schemm JK, Graham NE (1999) A statistical extended-range tropical forecast model based on the slow evolution of the Madden–Julian oscillation. *J Clim* 12:1918–1939. doi:[10.1175/1520-0442\(1999\)012<1918:ASERTF>2.0.CO;2](https://doi.org/10.1175/1520-0442(1999)012<1918:ASERTF>2.0.CO;2)
- Waliser DE, Lau KM, Stern W, Jones C (2003) Potential predictability of the Madden–Julian oscillation. *Bull Am Meteorol Soc* 84:33–50. doi:[10.1175/BAMS-84-1-33](https://doi.org/10.1175/BAMS-84-1-33)
- Wang B, Xie XS (1998) Coupled modes of the warm pool climate system. Part I: the role of air–sea interaction in maintaining Madden–Julian oscillation. *J Clim* 11:2116–2135. doi:[10.1175/1520-0442\(1998\)011<3010:EOCVSO>2.0.CO;2](https://doi.org/10.1175/1520-0442(1998)011<3010:EOCVSO>2.0.CO;2)
- Webster PJ et al (2002) The JASMINE pilot study. *Bull Am Meteorol Soc* 83:1603–1629. doi:[10.1175/BAMS-83-11-1603\(2002\)083<1603:TJPS>2.3.CO;2](https://doi.org/10.1175/BAMS-83-11-1603(2002)083<1603:TJPS>2.3.CO;2)
- Webster PJ, Lukas R (1992) TOGA-COARE: the coupled ocean–atmosphere response experiment. *Bull Am Meteorol Soc* 73:1377–1416. doi:[10.1175/1520-0477\(1992\)073<1377:TCTCOR>2.0.CO;2](https://doi.org/10.1175/1520-0477(1992)073<1377:TCTCOR>2.0.CO;2)
- Webster PJ, Hoyos C (2004) Prediction of monsoon rainfall and river discharge on 15–30 day time scales. *Bull Am Meteorol Soc* 85:1745–1765. doi:[10.1175/BAMS-85-11-1745](https://doi.org/10.1175/BAMS-85-11-1745)
- Wheeler M, Weickmann KM (2001) Real-time monitoring and prediction of modes of coherent synoptic to intraseasonal tropical variability. *Mon Weather Rev* 129:2677–2694. doi:[10.1175/1520-0493\(2001\)129<2677:RTMAPO>2.0.CO;2](https://doi.org/10.1175/1520-0493(2001)129<2677:RTMAPO>2.0.CO;2)
- Wolff JE, Maier-Reimer E, Legutzke S (1997) The hamburg ocean primitive equation model. Deutsches Klimarechenzentrum, Hamburg, Technical Report No. 13
- Woolnough SJ, Slingo JM, Hoskins BJ (2000) The relationship between convection and sea surface temperature on intraseasonal timescales. *J Clim* 13:2086–2104. doi:[10.1175/1520-0442\(2000\)013<2086:TRBCAS>2.0.CO;2](https://doi.org/10.1175/1520-0442(2000)013<2086:TRBCAS>2.0.CO;2)
- Woolnough SJ, Vitart F, Balmaseda M (2007) The role of the ocean in the Madden–Julian oscillation: sensitivity of an MJO forecast to ocean coupling. *Q J R Meteorol Soc* 133:117–128. doi:[10.1002/qj.4](https://doi.org/10.1002/qj.4)
- Zhang C (2005) Madden–Julian oscillation. *Rev Geophys* 43:RG2003. doi:[10.1029/2004RG000158](https://doi.org/10.1029/2004RG000158)